





Optimal control and ultimate bounds of 1:2 nonlinear quantum systemsJing-jun Zhu ^{1,2} Kaipeng Liu ² Xi Chen ^{3,4} and Stéphane Guérin ^{1,*}¹*Laboratoire Interdisciplinaire Carnot de Bourgogne, CNRS UMR 6303, Université de Bourgogne, Boîte Postale 47870, 21078 Dijon, France*²*International Center of Quantum Artificial Intelligence for Science and Technology and Department of Physics, Shanghai University, Shanghai 200444, China*³*Department of Physical Chemistry, University of the Basque Country UPV/EHU, Apartado 644, 48080 Bilbao, Spain*⁴*EHU Quantum Center, University of the Basque Country UPV/EHU, Barrio Sarriena, s/n, 48940 Leioa, Spain*

(Received 28 March 2023; accepted 11 September 2023; published 16 October 2023)

Using optimal control, we establish and link the ultimate bounds in time (referred to as the quantum speed limit) and energy of two- and three-level quantum nonlinear systems which feature 1:2 resonance. Despite the unreachable complete inversion, by using the Pontryagin maximum principle, we determine the optimal time, pulse area, or energy for a given arbitrary accuracy. We show that the third-order Kerr terms can be absorbed in the detuning in order to lock the dynamics to the resonance. In the two-level problem, we determine the nonlinear counterpart of the optimal π -pulse inversion for a given accuracy. In the three-level problem, we obtain an intuitive pulse sequence similar to the linear counterpart but with different shapes. We prove the (slow) logarithmic increasing of the optimal time as a function of the accuracy.

DOI: [10.1103/PhysRevA.108.042610](https://doi.org/10.1103/PhysRevA.108.042610)**I. INTRODUCTION**

The accurate control of quantum dynamics is at the core of the quantum world. Quantum control protocols have been developed in order to design specific shaped pulses, including composite [1–6], adiabatic [7–9], shortcut-to-adiabatic [10–13], and single-shot shaped-pulse [14–16] techniques. However, these protocols, even when accelerated compared to standard adiabatic passage, do not specifically control the time of operation, which can lead to severe obstructions to experimental implementation. In this context, optimal control theory (OCT) [17] has emerged as a powerful tool to mitigate intensities of pulses, allowing one to attain the ultimate time bound in the system, which is also interpreted as the quantum speed limit [18–21]. Besides numerical implementation of OCT, such as the monotonically convergent iteration algorithm [22–25], global Krotov method [26], Gradient ascent pulse engineering algorithm (GRAPE) [27], one can highlight the Pontryagin maximum principle (PMP) [28–32], which, transforming the initial infinite-dimensional control problem into a finite-dimensional problem, allows analytic derivation of the optimal controls (typically with respect to time or energy). One can also mention recent geometric approaches [33–35] treating simultaneously robust and optimal control.

The extension of quantum control techniques to nonlinear quantum systems relevant to describe Bose-Einstein condensation (BEC), e.g., when one considers the conversion from atomic to molecular BEC, leading to a so-called 1:2 Fermi resonance [36], is a nontrivial issue. The system has to be reinterpreted and analyzed with tools from classical mechanics, where the concept of integrability, without a counterpart

in the standard linear quantum physics, plays an important role [37,38]. When the system is integrable, adiabatic-passage techniques can be formulated with trajectories formed by the instantaneous (stable) elliptic fixed points defined at each value of the adiabatic parameters and continuously connected to the initial condition. Obstructions to classical adiabatic passage are given by the crossing of a separatrix [39–41]. In addition, for a two-level problem with a 1:2 resonance, the north pole of the generalized Bloch sphere (associated with the upper state and thus corresponding to a complete population transfer from the ground state) is unstable since it is associated with a hyperbolic fixed point in the classical phase-space representation [42]. This prevents adiabatic passage from being robust when it approaches the north pole. The system is not controllable at this point in the sense that the nonlinearity prevents reaching the upper state exactly [40]. However, one can approach it as closely as required, and inverse-engineering techniques [43,44] have been developed for that purpose.

Ultimate bounds, e.g., the quantum speed limit [19], can be defined via the minimization of a given cost (such as time, pulse area, or energy) determined from optimal control; their extension to nonlinear systems is an open question. The purpose of this work is to establish and link these ultimate bounds in terms of time and energy using optimal control. We present a complete study of optimal control via the PMP for the two- and three-level systems featuring a 1:2 resonance, considering the cost as time or energy. Since the complete inversion from the ground state is unreachable, we define the target with a given (arbitrary) accuracy.

Reference [32] considered optimal time in two-level systems for various constraints (fixed detuning and coupling). Here, we consider the more general problem of optimal time and energy without assuming a constant coupling. We

*sguer@u-bourgogne.fr

establish in this paper several results for nonlinear models featuring a 1:2 nonlinearity: (i) time or energy optimality, which induces a constant coupling for both two- and three-level systems (considering the generalized coupling for the latter case), (ii) asymptotic logarithmic scaling of the optimal pulse area (and, consequently, optimal time for a given coupling) as a function of the chosen accuracy for nonlinear two- and three-level models, and (iii) isomorphism between nonlinear three-level and two-level models and mapping of the nonlinear three-level model on the standard Bloch sphere (rather than the generalized drop-shaped Bloch sphere relevant for the nonlinear two-level problem).

Sections II and III are devoted to two- and three-states problems, respectively. We conclude in Sec. IV.

II. 1:2 NONLINEAR TWO-LEVEL MODEL

A. The model

The two-level model including second-order (with a 1:2 resonance) and third-order Kerr nonlinearities is characterized by following equations of motion [40]:

$$i\dot{\psi}_1 = \left[-\frac{\Delta}{3} + \Lambda_{11}|\psi_1|^2 + \Lambda_{12}|\psi_2|^2 \right] \psi_1 + \frac{\Omega}{\sqrt{2}} \psi_1^* \psi_2, \quad (1a)$$

$$i\dot{\psi}_2 = \left[\frac{\Delta}{3} + \Lambda_{21}|\psi_1|^2 + \Lambda_{22}|\psi_2|^2 \right] \psi_2 + \frac{\Omega}{2\sqrt{2}} \psi_1^2, \quad (1b)$$

where ψ_1 and ψ_2 are the state probability amplitudes, satisfying $|\psi_1|^2 + 2|\psi_2|^2 = 1$, which can vary in the respective ranges $|\psi_1|^2 \in [0, 1]$ and $|\psi_2|^2 \in [0, 1/2]$. The controls are time dependent: $\Delta \equiv \Delta(t)$ and $\Omega \equiv \Omega(t)$, representing the detuning and Rabi frequency, respectively. Here, Λ_{ij} ($i, j = 1, 2$) denote the third-order nonlinearities (in units of angular frequency), and $\Lambda_{21} = \Lambda_{12}$. Second-order nonlinearities appear in the form of the coupling. We will use units such that $\hbar = 1$.

We can describe the dynamics on a generalized non-linear Bloch sphere (see, e.g., [42,45]) by introducing the nonlinear coherences and the population inversion, respectively:

$$\eta_1 = \sqrt{2} \operatorname{Re}(\psi_1^2 \bar{\psi}_2), \quad \eta_2 = \sqrt{2} \operatorname{Im}(\psi_1^2 \bar{\psi}_2), \quad (2a)$$

$$\eta_3 = |\psi_2|^2 - \frac{1}{2}|\psi_1|^2, \quad \eta_3 \in \left[-\frac{1}{2}, \frac{1}{2}\right], \quad (2b)$$

leading to

$$|\psi_1|^2 = \frac{1}{2}(1 - 2\eta_3), \quad |\psi_2|^2 = \frac{1}{4}(1 + 2\eta_3). \quad (3)$$

The generalized 1:2 nonlinear Bloch sphere is characterized by the following surface equation:

$$\eta_1^2 + \eta_2^2 - \left(\frac{1}{2} - \eta_3\right)^2 \left(\frac{1}{2} + \eta_3\right) = 0. \quad (4)$$

The south and north poles correspond to $|\psi_1|^2 = 1$ and $|\psi_2|^2 = 0$ (i.e., $\eta_3 = -1/2$) and $|\psi_1|^2 = 0$ and $|\psi_2|^2 = 1/2$ (i.e., $\eta_3 = 1/2$), respectively. It was proved that $\eta_3 = 1/2$ is an unreachable (unstable) target with or without Kerr terms in [40,41]. Using Eq. (1), we have

$$\dot{\eta}_1 = (-\Delta + \Lambda_a - 2\Lambda_s|\psi_2|^2)\eta_2, \quad (5a)$$

$$\dot{\eta}_2 = \frac{\Omega}{2} \left(3\eta_3^2 - \eta_3 - \frac{1}{4} \right) + (\Delta - \Lambda_a + 2\Lambda_s|\psi_2|^2)\eta_1, \quad (5b)$$

$$\dot{\eta}_3 = \Omega\eta_2, \quad (5c)$$

with the effective third-order nonlinearities

$$\Lambda_s = 2\Lambda_{11} + \Lambda_{22}/2 - 2\Lambda_{12}, \quad \Lambda_a = 2\Lambda_{11} - \Lambda_{21}. \quad (6)$$

It can be seen that Λ_a can be trivially compensated by a static shift of the detuning, while the term proportional to Λ_s depends on the dynamical variable $|\psi_2|^2$. However, it was shown in [43] that one can lock the resonance using the freedom in the choice of the time dependance of Δ by incorporating the term $2\Lambda_s|\psi_2|^2$. Hence, we define the effective detuning (which includes a change in the sign of Δ for convenience):

$$\tilde{\Delta} = -\Delta + \Lambda_a - 2\Lambda_s|\psi_2|^2 = -\Delta + \Lambda_a - \Lambda_s\left(\frac{1}{2} + \eta_3\right), \quad (7)$$

such that the set (5) of differential equations features only the second-order nonlinearity:

$$\dot{\eta}_1 = \tilde{\Delta}\eta_2, \quad (8a)$$

$$\dot{\eta}_2 = \frac{\Omega}{2} \left(3\eta_3^2 - \eta_3 - \frac{1}{4} \right) - \tilde{\Delta}\eta_1, \quad (8b)$$

$$\dot{\eta}_3 = \Omega\eta_2. \quad (8c)$$

This generalizes the standard Bloch equations to the 1:2 nonlinear system with the detuning $\tilde{\Delta}$ (7) featuring an explicit (linear) dependance on η_3 via the effective third-order nonlinear term Λ_s . To determine the expression of optimal trajectories in this system, we apply the PMP, taking for the cost the time (time-optimal control) or the energy (energy-optimal control). The 1:2 nonlinear two-state time-optimal control was solved in [32], and we closely follow its derivation in order to apply it for the energy-optimal control and, in the next section, for the three-level problem.

To achieve a given transfer from a population $\eta_{3i} \equiv \eta_3(t_i)$ at the initial time t_i , we define the targeted final population $\eta_{3f} \equiv \eta_3(t_f) = \frac{1}{2} - \epsilon$ at the final time t_f , i.e., $|\psi_2(t_f)|^2 = \frac{1}{2}(1 - \epsilon)$. When one targets the upper state, the deviation ϵ will be taken to be small but different from zero since the second-order nonlinearity prevents reaching it exactly.

B. Time- and area-optimal control

Various situations were considered in [32]. Here, we particularly focus on the (almost) complete transfer from the ground state as a function of ϵ and will show that the minimum time (or pulse area) increases in a (slow) logarithmic way with respect to small deviations ϵ , or, reciprocally, that the deviation ϵ decreases exponentially with respect to the minimum time (or pulse area).

We consider the time-minimizing functional

$$J = \int_{t_i}^{t_f} dt. \quad (9)$$

The corresponding control (or pseudo) Hamiltonian from the set (8) of differential equations is (where we have added a constant p_0)

$$h_c = \tilde{\Delta}(\lambda_1\eta_2 - \lambda_2\eta_1) + \Omega \left[\frac{\lambda_2}{2} \left(3\eta_3^2 - \eta_3 - \frac{1}{4} \right) + \lambda_3\eta_2 \right], \quad (10)$$

with Hamiltonian's equation for the (dimensionless) costate $\Lambda = [\lambda_1, \lambda_2, \lambda_3]^\top$ gathering the conjugate momenta of η_1 , η_2 , and η_3 , respectively:

$$\dot{\lambda}_1 = -\frac{\partial h_c}{\partial \eta_1} = \lambda_2 \tilde{\Delta}, \quad (11a)$$

$$\dot{\lambda}_2 = -\frac{\partial h_c}{\partial \eta_2} = -\lambda_1 \tilde{\Delta} - \lambda_3 \Omega, \quad (11b)$$

$$\dot{\lambda}_3 = -\frac{\partial h_c}{\partial \eta_3} = -\frac{\lambda_2}{2} \Omega (6\eta_3 - 1) - \frac{\partial \tilde{\Delta}}{\partial \eta_3} (\lambda_1 \eta_2 - \lambda_2 \eta_1). \quad (11c)$$

In order to prevent an arbitrarily large field amplitude detrimental to experimental implementation, we impose a boundary on the field $\Omega \leq \Omega_0$ as a constraint. The maximization of h_c according to the PMP corresponds thus to the necessary condition

$$\frac{\partial h_c}{\partial \tilde{\Delta}} = 0, \quad (12)$$

i.e.,

$$\lambda_1 \eta_2 - \lambda_2 \eta_1 = 0. \quad (13)$$

This leads to the shape of the external field Ω ,

$$\Omega = \frac{2}{\lambda_2 (3\eta_3^2 - \eta_3 - \frac{1}{4}) + 2\lambda_3 \eta_2}, \quad (14)$$

from (10) and (13) and the fact that the system (10) is autonomous, i.e., $h_c = \text{const}$. In Eq. (14), we have renormalized $\lambda_2/h_c \rightarrow \lambda_2$ and $\lambda_3/h_c \rightarrow \lambda_3$ without loss of generality. Differentiating Eqs. (13) and (14) gives

$$\frac{\lambda_1}{2} \left(3\eta_3^2 - \eta_3 - \frac{1}{4} \right) + \lambda_3 \eta_1 = 0, \quad (15)$$

$$\dot{\Omega} = 0, \quad (16)$$

from which we conclude that Ω is constant, taken at its maximum $\Omega = \Omega_0$. Multiplying Eq. (14) by η_1 and Eq. (15) by η_2 also using (13), we obtain a linear system of equations for the variables λ_2 and λ_3 :

$$\lambda_2 \frac{\eta_1}{2} \left(3\eta_3^2 - \eta_3 - \frac{1}{4} \right) + \lambda_3 \eta_1 \eta_2 = \frac{\eta_1}{\Omega}, \quad (17a)$$

$$\lambda_2 \frac{\eta_1}{2} \left(3\eta_3^2 - \eta_3 - \frac{1}{4} \right) + \lambda_3 \eta_1 \eta_2 = 0 \quad (17b)$$

of determinant zero, which can give a solution when the inhomogeneous terms are zero, i.e., $\eta_1 = 0$. This implies $\lambda_1 = 0$ from Eq. (15) (for a nonconstant η_3), and $\dot{\eta}_1 = 0$ in Eq. (8a) gives $\tilde{\Delta} = 0$, i.e., for the original detuning Δ from (7),

$$\Delta = \Lambda_a - \Lambda_s \left(\frac{1}{2} + \eta_3 \right). \quad (18)$$

This leads to an optimal trajectory along the meridian connecting the south pole to the target near the north pole (of distance ϵ from it) in the (η_2, η_3) plane. The dynamics can be solved exactly from (8). For instance, when we consider a population transfer from the ground state (south pole), i.e., $\eta_{3i} = -1/2$, we obtain (taking $t_i = 0$)

$$\eta_3(t) = \tanh^2 \left(\frac{1}{2} \Omega_0 t \right) - \frac{1}{2}. \quad (19)$$

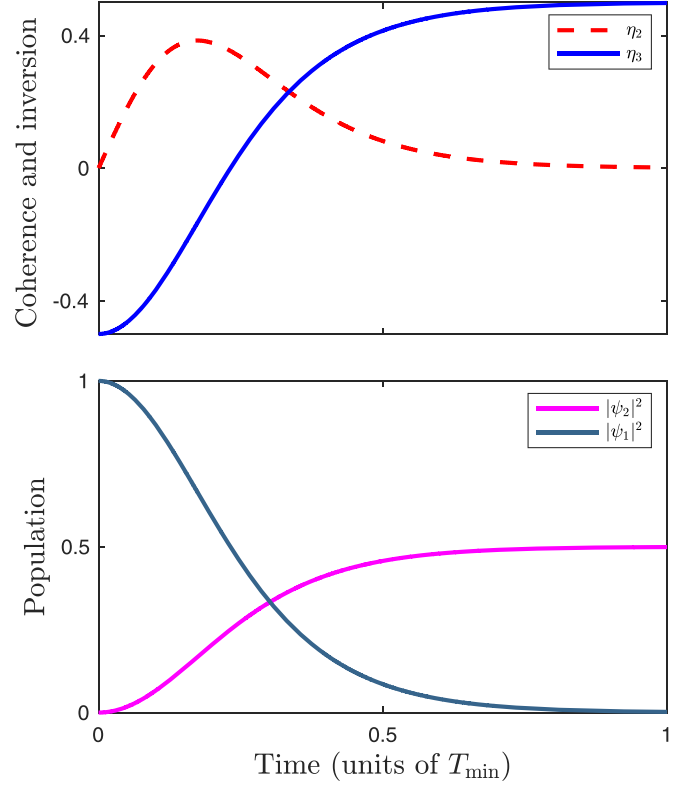


FIG. 1. Population (bottom) and coherence and population inversion (top) history, given by (19) and integration of (8b), governed by the time-optimal (constant) pulse Ω_0 for $\epsilon = 0.002$, giving $\mathcal{A} \approx 7.60$, i.e., $T_{\min} \approx 7.60/\Omega_0$.

From Eq. (14), taken at the initial time, we obtain $\Omega_0 = 2/\lambda_{2i}$ (independent of the initial value of $\lambda_{3,i}$). To obtain the explicit expression of the minimum time $T_{\min} = \min(t_f - t_i)$ for a given Ω_0 , we calculate the corresponding minimum pulse area by integrating (8c) using (4), which is fully determined by the (given) initial and final boundaries of η_3 ,

$$\mathcal{A}_{\min} \equiv \Omega_0 T_{\min} = \pm \int_{\eta_{3i}}^{\eta_{3f}} \frac{d\eta_3}{\sqrt{\left(\frac{1}{2} - \eta_3\right)^2 \left(\frac{1}{2} + \eta_3\right)}}. \quad (20)$$

The \pm sign ensures a non-negative pulse area; that is, the $+$ ($-$) sign corresponds to $\eta_{3i} < \eta_{3f}$ ($\eta_{3i} > \eta_{3f}$). Therefore, we consider $\eta_{3i} < \eta_{3f} = \frac{1}{2} - \epsilon$ and finally get the minimum time for given ϵ and Ω_0 ,

$$T_{\min} = \frac{2}{\Omega_0} \left| \operatorname{atanh} \sqrt{\frac{1}{2} + \eta_{3f}} - \operatorname{atanh} \sqrt{\frac{1}{2} + \eta_{3i}} \right|. \quad (21)$$

This gives, for the nonlinear final transfer probability from the ground state in optimal time T_{\min} ,

$$p = 2|\psi_2(T_{\min})|^2 = \tanh^2 \left(\frac{1}{2} \Omega_0 T_{\min} \right) = 1 - \epsilon. \quad (22)$$

We notice in the limit case of unbounded pulse amplitude a Dirac δ pulse, i.e., of infinite amplitude and zero duration with a finite area $\Omega_0 T_{\min}$ given by (21). The dynamics from the ground state is shown in Fig. 1 for $\epsilon = 0.002$. As expected, its trajectory is a curve along a meridian on the generalized drop-shaped Bloch sphere, as shown in Fig. 2.

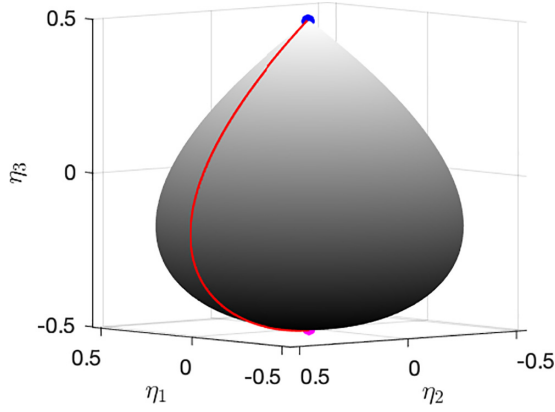


FIG. 2. Optimal trajectory obtained from time-optimal control of the nonlinear two-level model on the generalized drop-shaped Bloch sphere, which connects the initial (magenta dot) and target states, very close to the north pole (blue dot), defined by $\eta_3 = 1 - \epsilon$ ($\epsilon = 0.002$).

The minimum time T_{\min} can be used as the definition of the so-called quantum speed limit in this system, as suggested in [20]. In linear systems, the minimum time is given by $T_{\min, \text{lin.}}: \cos(\Omega_0 T_{\min, \text{lin.}}/2) = \frac{1}{2}\sqrt{1 - \eta_{3i}}\sqrt{1 - \eta_{3f}} + \frac{1}{2}\sqrt{1 + \eta_{3i}}\sqrt{1 + \eta_{3f}}$ [20,29], with $\eta_{3i} = -1$ for the ground state and $\eta_{3f} = 1$ for the excited state. In the nonlinear case we obtain $\tanh(\Omega_0 T_{\min}/2) = \sqrt{\frac{1}{2} + \eta_{3f}}$ for $\eta_{3i} = -1/2$ from Eq. (21).

We consider $\eta_{3i} = -1/2$ (south pole). The pulse area $\mathcal{A}_{\min} = \Omega_0 T_{\min}$ is given from Eq. (21) with its leading order for $\epsilon \rightarrow 0$:

$$\mathcal{A}_{\min} = 2 \operatorname{atanh} \sqrt{1 - \epsilon} \sim -\ln\left(\frac{\epsilon}{4}\right), \quad (23)$$

i.e., $\epsilon \sim 4e^{-\mathcal{A}_{\min}}$. We conclude that the minimum time (or pulse area) for the (almost complete) inversion increases in a (slow) logarithmic way with respect to small deviations ϵ , or, reciprocally, that the deviation ϵ decreases exponentially with respect to the minimum time (or pulse area). Figure 3 compares the pulse-area cost between the linear probability, $p_{\text{lin}} = \sin^2(\Omega_0 T_{\min}/2)$, and the nonlinear probability (22). One can observe that the nonlinearity weakly affects the transfer for small transfers ($\epsilon \rightarrow 1$).

C. Energy-optimal control

We consider the cost functional for the energy-optimal control

$$J \equiv E = \hbar \int_{t_i}^{t_f} \Omega^2(t) dt. \quad (24)$$

In this case, we can rewrite the control Hamiltonian (in units such that $\hbar = 1$) as

$$h_c = \tilde{\Delta}(\lambda_1 \eta_2 - \lambda_2 \eta_1) + \Omega \left[\frac{\lambda_2}{2} \left(3\eta_3^2 - \eta_3 - \frac{1}{4} \right) + \lambda_3 \eta_2 \right] - p_0 \Omega^2, \quad (25)$$

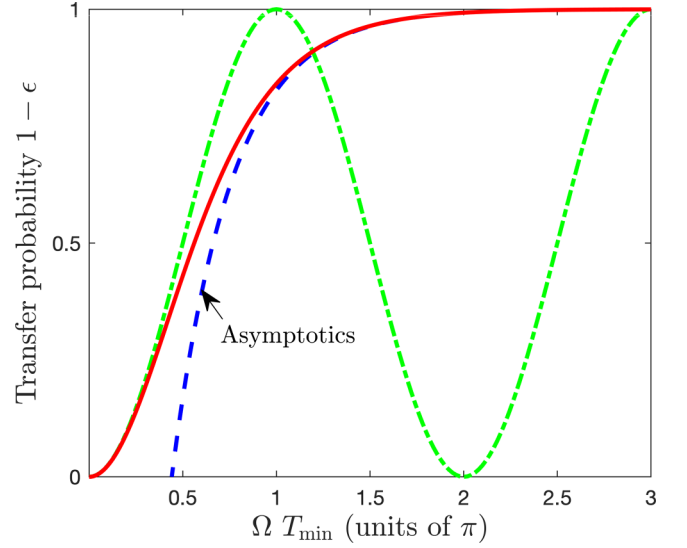


FIG. 3. Population-transfer probability $1 - \epsilon$ as a function of the optimal pulse area for the linear $p_{\text{lin}} = \sin^2(\Omega_0 T_{\min}/2)$ (green dotted-dashed line) and nonlinear (red solid line) two-level models. The asymptotics (23) of the probability (blue dashed line) shows its accuracy when $\epsilon \rightarrow 0$.

with the standard choice $p_0 = 1/2$. In this case, the costate has the angular frequency unit. After applying the PMP,

$$\frac{\partial h_c}{\partial \tilde{\Delta}} = 0, \quad \frac{\partial h_c}{\partial \Omega} = 0, \quad (26)$$

we obtain $\lambda_1 \eta_2 - \lambda_2 \eta_1 = 0$ and

$$\Omega = \frac{\lambda_2}{2} \left(3\eta_3^2 - \eta_3 - \frac{1}{4} \right) + \lambda_3 \eta_2. \quad (27)$$

The control Hamiltonian can be rewritten as

$$h_c = \frac{1}{2} \Omega^2, \quad (28)$$

leading to a constant coupling $\Omega = \Omega_0 = \sqrt{2h_c}$. Like for the time-optimum case, we obtain $\eta_1 = 0$, $\lambda_1 = 0$, $\tilde{\Delta} = 0$, and thus the same dynamics as in Fig. 1. We also derive Eq. (21) but interpret it differently; that is, for a given time of interaction $T = t_f - t_i$, we determine the minimum Ω_0 :

$$\Omega_{0, \min} = \frac{2}{T} \left| \operatorname{atanh} \sqrt{\frac{1}{2} + \eta_{3f}} - \operatorname{atanh} \sqrt{\frac{1}{2} + \eta_{3i}} \right|, \quad (29)$$

leading to the minimum energy

$$E_{\min} = \hbar \Omega_{0, \min}^2 T = \hbar \mathcal{A}_{\min}^2 / T \quad (30)$$

corresponding to the minimum area given by (29): $\mathcal{A}_{\min} = \Omega_{0, \min} T = 2 \left| \operatorname{atanh} \sqrt{\frac{1}{2} + \eta_{3f}} - \operatorname{atanh} \sqrt{\frac{1}{2} + \eta_{3i}} \right|$.

III. 1:2 NONLINEAR THREE-LEVEL Λ MODEL

A. The model

The equations of motion for the three-level Raman model (forming a Λ system), including the second- and third-order

nonlinearities, read

$$i\dot{\psi}_1 = K_1\psi_1 + \Omega_p\psi_1^*\psi_2, \quad (31a)$$

$$i\dot{\psi}_2 = K_2\psi_2 + \Delta_P\psi_2 + \frac{\Omega_p}{2}\psi_1^2 + \frac{\Omega_s}{2}\psi_3, \quad (31b)$$

$$i\dot{\psi}_3 = K_3\psi_3 + \frac{\Omega_s}{2}\psi_2 + (\Delta_P - \Delta_S)\psi_3, \quad (31c)$$

where Ω_p and Ω_s are the time-dependent pump and Stokes fields, respectively, Δ_P is the one-photon detuning associated with the pump coupling, and $\Delta_P - \Delta_S$ is the two-photon detuning associated with the Raman process. The second-order 1:2 nonlinearity appears here through the pump coupling. This is typically the situation for the two-color photoassociation process [36]. The third-order nonlinearities K_j ($j = 1, 2, 3$) can be absorbed in the definition of the detunings and the change of phases $\psi_1 \rightarrow \psi_1 e^{-i\gamma}$ and $\psi_{2,3} \rightarrow \psi_{2,3} e^{-2i\gamma}$, $\dot{\gamma} = K_1$, $\Delta_P = 2K_1 - K_2$, and $\Delta_S = K_3 - K_2$, in order to lock the (one- and two-photon) resonances [43]:

$$i\dot{\psi}_1 = \Omega_p\psi_1^*\psi_2, \quad (32a)$$

$$i\dot{\psi}_2 = \frac{\Omega_p}{2}\psi_1^2 + \frac{\Omega_s}{2}\psi_3, \quad (32b)$$

$$i\dot{\psi}_3 = \frac{\Omega_s}{2}\psi_2. \quad (32c)$$

The amplitude probabilities satisfy $|\psi_1|^2 + 2(|\psi_2|^2 + |\psi_3|^2) = 1$. We decompose the components into real and imaginary parts, $\psi_i = x_i + iy_i$ ($i = 1, 2, 3$), and assume real Rabi frequencies, which allows us to separate the original problem into two disjoint dynamics that emerge according to the real and imaginary parts of the initial state. We consider the initial state ψ_1 to be real, $x_1(t_i) = 1$, and we get the equations of motion from (32):

$$\dot{x}_1 = \Omega_p x_1 y_2, \quad (33a)$$

$$\dot{y}_2 = -\frac{\Omega_s}{2}x_3 - \frac{\Omega_p}{2}x_1^2, \quad (33b)$$

$$\dot{x}_3 = \frac{\Omega_s}{2}y_2. \quad (33c)$$

This system of equations can be analyzed using an isomorphism with the nonlinear two-level problem similarly to the linear problem [46] (see the Appendix). One can also show the incomplete transfer between the two ground states for finite pulse areas. We, however, prefer to keep the original coordinates for solving the problem.

Without loss of generality, we can parametrize the dynamics with the two dynamical angles $\theta(t) \in [0, \pi]$ and $\phi(t) \in [0, 2\pi[$:

$$x_1 = \cos \phi \cos \theta, \quad (34a)$$

$$y_2 = -\frac{1}{\sqrt{2}} \sin \phi, \quad (34b)$$

$$x_3 = -\frac{\cos \phi \sin \theta}{\sqrt{2}}, \quad (34c)$$

which satisfies the normalization condition $x_1^2 + 2(y_2^2 + x_3^2) = 1$. Inserting definition (34) into Eqs. (33) leads

to

$$\dot{\phi} = \frac{\Omega_p \cos \phi \cos^2 \theta}{\sqrt{2}} - \frac{\Omega_s \sin \theta}{2}, \quad (35a)$$

$$\dot{\theta} = \frac{\sin \phi \sin \theta}{\cos \phi \cos \theta} \left(\frac{\Omega_s}{2 \sin \theta} + \frac{\Omega_p \cos \phi \cos^2 \theta}{\sqrt{2}} - \frac{\Omega_s \sin \theta}{2} \right), \quad (35b)$$

which, by inversion, provide the shape of the fields as a function of the angles:

$$\Omega_s = 2(\dot{\theta} \cot \phi \cos \theta - \dot{\phi} \sin \theta), \quad (36a)$$

$$\Omega_p = \sqrt{2} \left(\frac{\dot{\phi}}{\cos \phi} + \frac{\dot{\theta} \tan \theta}{\sin \phi} \right). \quad (36b)$$

We define the target state in the vicinity of state 3:

$$|x_3(t_f)|^2 = \frac{1}{2}(1 - \epsilon), \quad (37)$$

where ϵ is, as in the two-level case, a small deviation due to the incomplete population transfer in such a nonlinear system [43]. To determine the expression of the optimal trajectories from the ground state to the target state (for a given ϵ), we apply the PMP, taking for the cost the time or the energy.

B. Time-optimal control

1. Definition

We consider the time-minimizing cost functional (9) and impose, like in the two-level case, the constraint of bounded pulses amplitudes:

$$\Omega_p^2 + \Omega_s^2 \leq \Omega_0^2. \quad (38)$$

The control Hamiltonian reads (where we have added a constant p_0)

$$H_c = \lambda_\phi \dot{\phi} + \lambda_\theta \dot{\theta} \quad (39)$$

$$= \lambda_\phi \left(\frac{\Omega_p \cos \phi \cos^2 \theta}{\sqrt{2}} - \frac{\Omega_s \sin \theta}{2} \right) + \lambda_\theta \left(\frac{\Omega_s \cos \theta \tan \phi}{2} + \frac{\Omega_p \cos \theta \sin \theta \sin \phi}{\sqrt{2}} \right), \quad (40)$$

where $\lambda_{\phi, \theta}$ are the components of the (dimensionless) costate $\Lambda = [\lambda_\phi, \lambda_\theta]^T$ with the dynamics

$$\dot{\lambda}_\phi = -\frac{\partial H_c}{\partial \phi} = \frac{\lambda_\phi \Omega_p \sin \phi \cos^2 \theta}{\sqrt{2}} - \lambda_\theta \left(\frac{\Omega_s \cos \theta}{2 \cos^2 \phi} + \frac{\Omega_p \sin 2\theta \cos \phi}{2\sqrt{2}} \right), \quad (41a)$$

$$\dot{\lambda}_\theta = -\frac{\partial H_c}{\partial \theta} = \lambda_\phi \left(\frac{\Omega_p \cos \phi \sin 2\theta}{\sqrt{2}} + \frac{\Omega_s \cos \theta}{2} \right) + \lambda_\theta \left(\frac{\Omega_s \sin \theta \tan \phi}{2} - \frac{\Omega_p \cos 2\theta \sin \phi}{\sqrt{2}} \right). \quad (41b)$$

Without loss of the generality, we can consider the control functions satisfying constraint (38) as follows:

$$\Omega_p = \Omega_m(t) \cos \beta(t), \quad \Omega_s = \Omega_m(t) \sin \beta(t), \quad (42)$$

with the condition

$$\Omega_s^2 + \Omega_p^2 = \Omega_m^2 \leq \Omega_0^2. \quad (43)$$

Constraint (38) is thus transferred to condition (43) (which is independent of β). The PMP maximization of H_c is thus reduced to the necessary condition

$$\frac{\partial H_c}{\partial \beta} = 0, \quad (44)$$

which gives

$$\frac{\partial H_c}{\partial \beta} = \frac{\partial \Omega_p}{\partial \beta} H_1 + \frac{\partial \Omega_s}{\partial \beta} H_2 = -H_1 \sin \beta + H_2 \cos \beta = 0, \quad (45)$$

where

$$H_1 = \frac{\lambda_\phi \cos \phi \cos^2 \theta}{\sqrt{2}} + \frac{\lambda_\theta \sin 2\theta \sin \phi}{2\sqrt{2}}, \quad (46a)$$

$$H_2 = \frac{\lambda_\theta \cos \theta \tan \phi}{2} - \frac{\lambda_\phi \sin \theta}{2}. \quad (46b)$$

We then deduce

$$\cos \beta = \frac{H_1}{\sqrt{H_1^2 + H_2^2}}, \quad \sin \beta = \frac{H_2}{\sqrt{H_1^2 + H_2^2}}. \quad (47)$$

Substituting Eq. (47) in Eq. (39), we obtain

$$H_c = \Omega_m \sqrt{H_1^2 + H_2^2}, \quad (48)$$

from which we conclude that the control Hamiltonian is maximum for $\Omega_m = \Omega_0$, i.e., when the maximum of (38) is reached at all times.

2. Numerics

We first determine the systematic landscape of the time T to reach the target (for a given ϵ) by solving the set of equations (35) and (41) with the controls (42) and $\Omega_m = \Omega_0$ rewritten as a function of the angles and the costate components via (47) and (46) as a function of parameters $\lambda_{\phi,i}$ and $\lambda_{\theta,i}$, which, with $\theta_i = 0$ and $\phi_i = 0$, form the set of initial conditions. The landscape is shown in Fig. 4, where the white areas corresponds to the absence of a solution reaching the given target in the prescribed interval. Figure 4 shows an infinite set of initial $\lambda_{\phi,i}$ and $\lambda_{\theta,i}$ forming two straight (symmetric) lines that lead to the same minimum $T_{\min} \approx 7.4/\Omega_0$.

The four quadrants give all the possible respective signs of the controls. The controls are both positive when the initial values $\lambda_{\phi,i}$ and $\lambda_{\theta,i}$ are taken to be positive. In order to determine a more accurate value of the optimum, we choose a certain value of $\lambda_{\phi,i}$ (e.g., $\lambda_{\phi,i} = 1.85$) and run an optimal procedure leading to the (positive) value $\lambda_{\theta,i} \approx 0.45266$ corresponding to the minimum time (using a Nelder-Mead simplex algorithm as described in [47]).

Figure 5 shows, as a function of ϵ , the minimum time via the minimum generalized pulse area defined as $\mathcal{A}_{\min} = \int_0^{T_{\min}} dt \sqrt{\Omega_p^2 + \Omega_s^2} = T_{\min} \Omega_0$. It exhibits a logarithmic decreasing behavior similar to the two-level case. This suggests the following ansatz for the population inspired by the two-level problem and the behavior of the optimal pulse area in Fig. 5 (taking $t_i = 0$):

$$y_2^2 + x_3^2 \approx \frac{1}{2} \tanh^2 \left(\frac{\Omega_0}{\sqrt{2}} t \right), \quad (49)$$

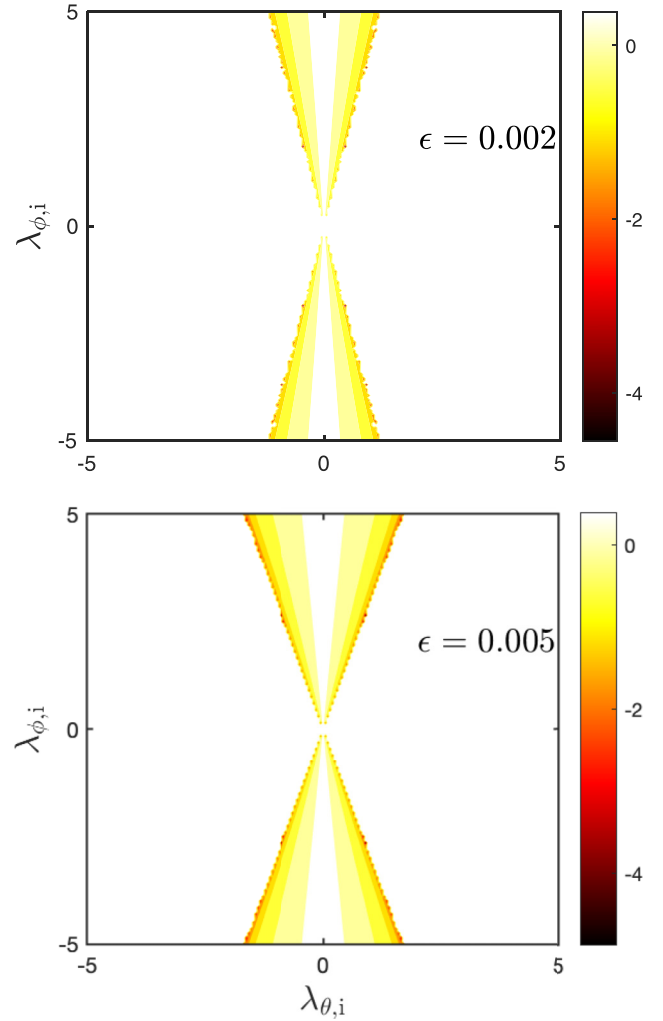


FIG. 4. Contour plot for $\log_{10}(T - T_{\min})$ as a function of dimensionless $\lambda_{\phi,i}$ and $\lambda_{\theta,i}$ when the dynamics reaches the targeted transfer for a given ϵ . The transfer time is determined in a given range $T \in [0, \hat{T}]$ (taken here as $\hat{T} = 15/\Omega_0$). The white areas mean that there is no transfer time found in the prescribed interval. We obtain $T_{\min} \approx 7.40/\Omega_0$ for $\epsilon = 0.002$ (top) and $T_{\min} \approx 6.78/\Omega_0$ for $\epsilon = 0.005$ (bottom) along the dark straight lines.

which fits well the numerics of the dynamics shown in Fig. 6 but slightly overestimates the accuracy (of the order of ϵ). The boundary at $t_f = T_{\min}$ gives the asymptotic expansion for small ϵ (with $y_{2f}^2 \ll x_{3f}^2$):

$$y_{2f}^2 + x_{3f}^2 \approx \frac{1}{2}(1 - \epsilon) \sim \frac{1}{2}(1 - 4e^{-\sqrt{2}\mathcal{A}_{\min}}), \quad (50)$$

i.e.,

$$\mathcal{A}_{\min} \sim -\frac{1}{\sqrt{2}}(\ln \epsilon - \ln 4). \quad (51)$$

We notice that the resulting logarithmic scaling with respect to ϵ is the same as the scaling of the fit determined from Fig. 5. The absolute value is different due to the systematic error of (49) mentioned above.

The dynamics and controls of Fig. 6 show an intuitive sequence of pulses with a large transient population in the upper state, similar to the linear case, which features pulses of

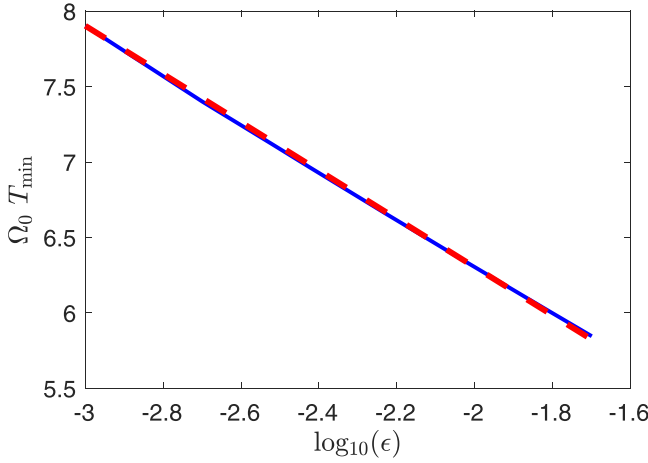


FIG. 5. Optimal pulse area (blue solid line) as a function of ϵ (in a logarithmic scale) for $\lambda_{\phi_i} = 1.85$ and the resulting optimum λ_{θ_i} and logarithmic fit of the asymptotics for small ϵ : $\mathcal{A}_{\min} = \Omega_0 T_{\min} \sim -(\ln \epsilon)/\sqrt{2} + 3$ (red dashed line).

explicit form $\cos - \sin$ [29,48]. Figure 7 shows the trajectory in the angle ϕ, θ space corresponding to the optimal nonlinear solution for $\epsilon = 0.002$; it is compared to the optimal solution of the linear problem.

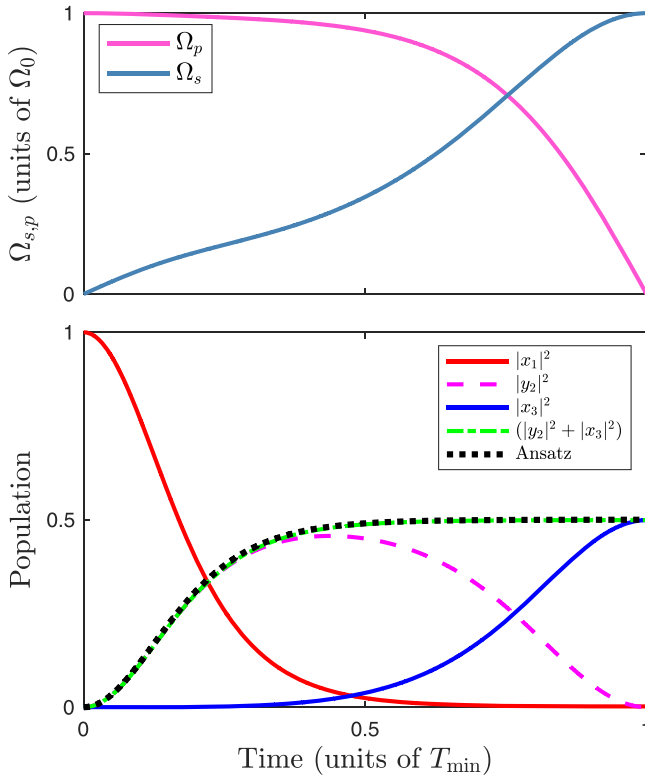


FIG. 6. Optimal pulse shapes (36) in units of Ω_0 with $\epsilon = 0.002$, $\lambda_{\phi_i} = 1.85$, and $\lambda_{\theta_i} \approx 0.45266$ operating in minimum time $T_{\min} \approx 7.40/\Omega_0$ (top) and the resulting population history and the ansatz (49) (bottom).

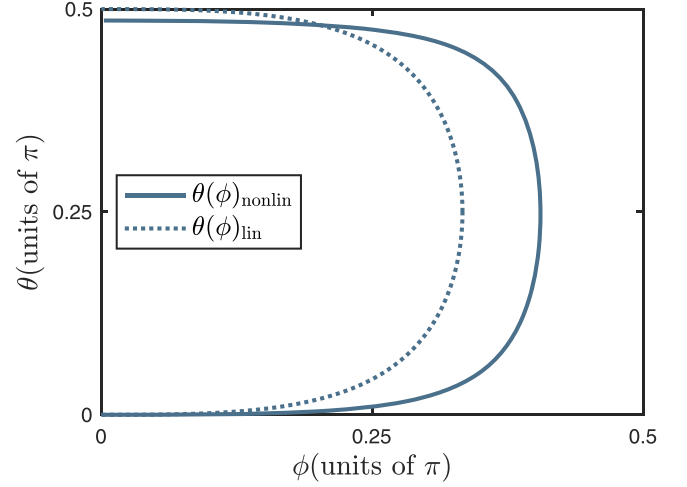


FIG. 7. Trajectories in the ϕ, θ space of the optimal nonlinear solution corresponding to the dynamics shown in Fig. 6 (solid line) and the optimal solution of the linear model (dotted line).

C. Energy-optimal control

For the energy optimization, we use the cost functional

$$J \equiv E = \hbar \int_{t_i}^{t_f} (\Omega_p^2 + \Omega_s^2) dt. \quad (52)$$

We derive the control Hamiltonian (using the standard value $p_0 = 1/2$):

$$\begin{aligned} H_c &= \lambda_\phi \dot{\phi} + \lambda_\theta \dot{\theta} - p_0 (\Omega_p^2 + \Omega_s^2) \\ &= \lambda_\phi \left(\frac{\Omega_p \cos \phi \cos^2 \theta}{\sqrt{2}} - \frac{\Omega_s \sin \theta}{2} \right) \\ &\quad + \lambda_\theta \left(\frac{\Omega_s \cos \theta \tan \phi}{2} + \frac{\Omega_p \cos \theta \sin \theta \sin \phi}{\sqrt{2}} \right) \\ &\quad - \frac{1}{2} (\Omega_p^2 + \Omega_s^2). \end{aligned} \quad (53)$$

The PMP $\frac{\partial H_c}{\partial \Omega_p} = 0$ and $\frac{\partial H_c}{\partial \Omega_s} = 0$ leads to the pulse shape:

$$\Omega_p = \frac{\lambda_\phi \cos \phi \cos^2 \theta}{\sqrt{2}} + \frac{\lambda_\theta \sin 2\theta \sin \phi}{2\sqrt{2}}, \quad (54a)$$

$$\Omega_s = \frac{\lambda_\theta \cos \theta \tan \phi}{2} - \frac{\lambda_\phi \sin \theta}{2}, \quad (54b)$$

and

$$H_c = \frac{1}{2} (\Omega_p^2 + \Omega_s^2), \quad (55)$$

which is constant as before, i.e., $\Omega_p^2 + \Omega_s^2 = \Omega_0^2$. The dynamics of the components of the (angular frequency unit) costate $\Lambda = [\lambda_\phi, \lambda_\theta]^T$ is still given by (41). We thus obtain the same dynamics shown in Fig. 6 as in the time-optimal control but for a given time of interaction $T = t_f - t_i$ (instead of T_{\min}). The corresponding optimal generalized pulse area \mathcal{A}_{\min} is determined from Fig. 5 for a given ϵ : $\mathcal{A}_{\min} \approx -\ln(\epsilon)/\sqrt{2} + 3$, and we deduce the corresponding $\Omega_{0,\min} = \mathcal{A}_{\min}/T$. The minimum energy is then

$$E_{\min} = \hbar \Omega_{0,\min}^2 T = \hbar \mathcal{A}_{\min}^2 / T. \quad (56)$$

IV. CONCLUSION

In this paper, we determined the ultimate bounds in terms of optimal time and optimal energy for the two-level and Raman three-level problems featuring a 1:2 nonlinear resonance when an accurate (but not strictly complete) population transfer is targeted. In both cases, we incorporated the third-order Kerr terms in the detuning locking the dynamics to the resonance at all times. In the two-level system, we showed the equivalence of the dynamics for the optimal time or energy, given by a resonant and constant pulse, as is the case for the linear problem. The behavior of the resonant nonlinear dynamics is qualitatively different from the linear one: the complete inversion is only (exponentially) asymptotic instead of Rabi oscillations of the linear problem (see Fig. 3). The optimal time features an asymptotic logarithmic increasing as a function of the accuracy. For the three-level problem, the optimal solution can be obtained only numerically. However, we fitted it using the similar results of the two-level problem. In this case, the generalized pulse area is constant. We determined the shape of the individual pulses featuring an intuitive pump-Stokes sequence, like in the linear case but with different shapes. We also obtained an asymptotic logarithmic increasing of the optimal time as a function of the accuracy.

The finding of the ultimate bounds (time or energy) for nonlinear systems provides an important benchmark. The issue of robustness of the process will have to be considered in future analysis involving optimal inverse engineering [34] since the (almost) complete transfer is very unstable when the resonance is not perfectly satisfied (see Fig. 1 of Ref. [40]). This is also the case for two-level adiabatic transfer [42]. We notice that this instability does not exist when only third-order nonlinearities apply.

ACKNOWLEDGMENTS

We acknowledge support from the EUR-EIPHI Graduate School (17-EURE-0002) and from the European Union's Horizon 2020 research and innovation program under Marie Skłodowska-Curie Grant No. 765075 (LIMQUET); France 2030 ANR-22-CMAS-0001 QuanTEdu-France. X.C. acknowledges EU FET Open Grant EPIQUS (Grant No. 899368); the Basque Government through Grant No. IT1470-22; the project grant PID2021-126273NB-I00 funded by MCIN/AEI/10.13039/501100011033 and by "ERDF A way of making Europe" and "ERDF Invest in your Future" and ayudas para contratos Ramon y Cajal-2015-2020 (RYC-2017-22482).

APPENDIX: ISOMORPHISM BETWEEN NON-LINEAR THREE-LEVEL AND TWO-LEVEL MODELS

The three-level problem (33) can be rewritten as

$$\dot{x}_1 = -Px_1z_2, \quad (\text{A1a})$$

$$\dot{z}_2 = Sz_3 + Px_1^2, \quad (\text{A1b})$$

$$\dot{z}_3 = -Sz_2, \quad (\text{A1c})$$

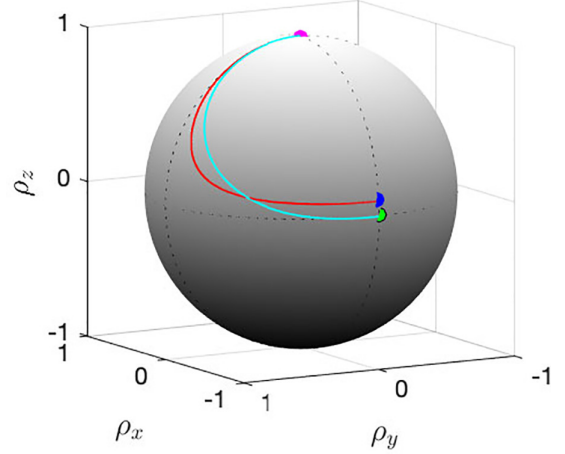


FIG. 8. Trajectories obtained from the optimal time of nonlinear (red line) and linear (cyan line) three-level models on the standard Bloch sphere, which connect the initial state (magenta dot) to the target state (blue and green dots, respectively). Here, we take the final state $|x_3(t_f)|^2 = (1 - \epsilon)/2$ ($\epsilon = 0.01$) for the nonlinear problem.

with $z_2 = -y_2\sqrt{2}$, $z_3 = x_3\sqrt{2}$, $P = \Omega_p/\sqrt{2}$, $S = \Omega_s/2$, and the normalization condition $x_1^2 + z_2^2 + z_3^2 = 1$. We assume that P and S are real and that $x_1(t_i) = 1$. It can be reinterpreted as a density "matrix" formulation on the Bloch sphere:

$$\frac{d}{dt} \begin{bmatrix} \rho_z \\ \rho_y \\ \rho_x \end{bmatrix} = \begin{bmatrix} 0 & -P\rho_z & 0 \\ P\rho_z & 0 & S \\ 0 & -S & 0 \end{bmatrix} \begin{bmatrix} \rho_z \\ \rho_y \\ \rho_x \end{bmatrix}, \quad (\text{A2})$$

with $\rho_z = x_1 = \rho_{11} - \rho_{22} = |a_1|^2 - |a_2|^2$, $\rho_y = z_2 = i(\rho_{21} - \rho_{12}) = 2\text{Im}(a_1\bar{a}_2)$, $\rho_x = z_3 = \rho_{21} + \rho_{12} = 2\text{Re}(a_1\bar{a}_2)$, and $\rho_{ij} = a_i\bar{a}_j$ for a nonlinear two-level problem

$$H_{2,nl} = \frac{1}{2} \begin{bmatrix} -S & P(|a_1|^2 - |a_2|^2) \\ P(|a_1|^2 - |a_2|^2) & S \end{bmatrix}, \quad (\text{A3})$$

with $i\frac{d}{dt}[a_1 \ a_2]^T = H_{2,nl}[a_1 \ a_2]^T$ and the normalization $|a_1|^2 + |a_2|^2 = 1$. As a consequence, the nonlinear three-level problem (A1) is isomorphic to the above nonlinear two-state problem (A3). The nonlinearity which appears here is not the one usually encountered for 1:2 resonance (1). We obtain a similar isomorphic relation for linear problems [46]. We can see that the standard Bloch sphere (i.e., not the generalized drop-shaped one) is involved in this problem.

As a consequence, the transfer is, at the final time t_f , complete, $|z_3(t_f)| = 1$, i.e., $\rho_x(t_f) = \pm 1$, when, in the counterpart two-state problem, from the initial state $\rho_{11}(t_i) = 1$, the superposition of the state of maximal coherence is produced: $\rho_{12}(t_f) = \rho_{21}(t_f) = \pm 1/2$. This shows a qualitative behavior similar to that for its linear analog, as shown in Fig. 8.

The general solution of the two-state problem (A3) can be parametrized by three angles in general:

$$\begin{bmatrix} a_1 \\ a_2 \end{bmatrix} = \begin{bmatrix} \cos(\theta/2) \\ \sin(\theta/2)e^{-i\varphi} \end{bmatrix} e^{-i\gamma}, \quad (\text{A4})$$

and the Schrödinger equation leads to the set of equations

$$\dot{\theta} = P \cos \theta \sin \varphi, \quad (\text{A5a})$$

$$\dot{\varphi} = S + P \frac{\cos^2 \theta}{\sin \theta} \cos \varphi, \quad (\text{A5b})$$

$$\dot{\gamma} = \frac{1}{2}(-S + P \cos \theta \tan(\theta/2) \cos \varphi). \quad (\text{A5c})$$

One can solve Eq. (A5a) exactly [for any $P(t)$ and $S(t)$]:

$$\tan(\theta/2) = \tanh \left[\frac{1}{2} \int_{t_i}^t P(s) \sin \varphi(s) ds \right]. \quad (\text{A6})$$

This shows that, in order to have a complete transfer from state 1 to state 3 in the original model, i.e., $\theta(t_i) = 0$ and $\theta(t_f) = \pi/2$, one needs an infinite pulse area of $P(t)$. This contrasts with the linear model, in which a complete population transfer is possible for finite pulse areas [29].

-
- [1] M. H. Levitt, Composite pulses, *Prog. Nucl. Magn. Reson. Spectrosc.* **18**, 61 (1986).
- [2] S. Wimperis, Broadband, narrowband, and passband composite pulses for use in advanced NMR experiments, *J. Magn. Reson. Ser. A* **109**, 221 (1994).
- [3] B. T. Torosov, S. Guérin, and N. V. Vitanov, High-fidelity adiabatic passage by composite sequences of chirped pulses, *Phys. Rev. Lett.* **106**, 233001 (2011).
- [4] J. A. Jones, Designing short robust NOT gates for quantum computation, *Phys. Rev. A* **87**, 052317 (2013).
- [5] S. S. Ivanov, B. T. Torosov, and N. V. Vitanov, High-fidelity quantum control by polychromatic pulse trains, *Phys. Rev. Lett.* **129**, 240505 (2022).
- [6] Z. Shi, C. Zhang, D. Ran, Y. Xia, R. Ianculescu, A. Friedman, X. X. Yi, and S. Zheng, Composite pulses for high fidelity population transfer in three-level systems, *New J. Phys.* **24**, 023014 (2022).
- [7] N. V. Vitanov, A. A. Rangelov, B. W. Shore, and K. Bergmann, Stimulated Raman adiabatic passage in physics, chemistry, and beyond, *Rev. Mod. Phys.* **89**, 015006 (2017).
- [8] K. Bergmann *et al.*, Roadmap on STIRAP applications, *J. Phys. B* **52**, 202001 (2019).
- [9] G. Dridi, S. Guérin, V. Hakobyan, H. R. Jauslin, and H. Eleuch, Ultrafast stimulated Raman parallel adiabatic passage by shaped pulses, *Phys. Rev. A* **80**, 043408 (2009).
- [10] X. Chen, I. Lizuain, A. Ruschhaupt, D. Guéry-Odelin, and J. G. Muga, Shortcut to adiabatic passage in two- and three-level atoms, *Phys. Rev. Lett.* **105**, 123003 (2010).
- [11] A. Ruschhaupt, X. Chen, D. Alonso, and J. G. Muga, Optimally robust shortcuts to population inversion in two-level quantum systems, *New J. Phys.* **14**, 093040 (2012).
- [12] D. Guéry-Odelin, A. Ruschhaupt, A. Kiely, E. Torrontegui, S. Martínez-Garaot, and J. G. Muga, Shortcuts to adiabaticity: Concepts, methods, and applications, *Rev. Mod. Phys.* **91**, 045001 (2019).
- [13] J. Zhu and X. Chen, Fast-forward scaling of atom-molecule conversion in Bose-Einstein condensates, *Phys. Rev. A* **103**, 023307 (2021).
- [14] D. Daems, A. Ruschhaupt, D. Sugny, and S. Guérin, Robust quantum control by a single-shot shaped pulse, *Phys. Rev. Lett.* **111**, 050404 (2013).
- [15] L. Van-Damme, D. Schraft, G. T. Genov, D. Sugny, T. Halfmann, and S. Guérin, Robust not gate by single-shot-shaped pulses, *Phys. Rev. A* **96**, 022309 (2017).
- [16] X. Laforgue, X. Chen, and S. Guérin, Robust stimulated Raman exact passage using shaped pulses, *Phys. Rev. A* **100**, 023415 (2019).
- [17] C. P. Koch, U. Boscain, T. Calarco, G. Dirr, S. Filipp, S. J. Glaser, R. Kosloff, S. Montangero, T. Schulte-Herbrüggen, D. Sugny, and F. K. Wilhelm, Quantum optimal control in quantum technologies. Strategic report on current status, visions and goals for research in Europe, *EPJ Quantum Technol.* **9**, 19 (2022).
- [18] T. Caneva, M. Murphy, T. Calarco, R. Fazio, S. Montangero, V. Giovannetti, and G. E. Santoro, Optimal control at the quantum speed limit, *Phys. Rev. Lett.* **103**, 240501 (2009).
- [19] G. C. Hegerfeldt, Driving at the quantum speed limit: Optimal control of a two-level system, *Phys. Rev. Lett.* **111**, 260501 (2013).
- [20] M. R. Frey, Quantum speed limits - primer, perspectives, and potential future directions, *Quantum Inf. Process.* **15**, 3919 (2016).
- [21] F-Q. Dou, J. Liu, and L.-B. Fu, Fast quantum driving in two-level systems with interaction and nonlinear sweep, *Phys. Rev. A* **98**, 022102 (2018).
- [22] W. Zhu, J. Botina, and H. Rabitz, Rapidly convergent iteration methods for quantum optimal control of population, *J. Chem. Phys.* **108**, 1953 (1998).
- [23] W. Zhu and H. Rabitz, Noniterative algorithms for finding quantum optimal controls, *J. Chem. Phys.* **110**, 7142 (1999).
- [24] J. Ruths and J. Lia, A multidimensional pseudospectral method for optimal control of quantum ensembles, *J. Chem. Phys.* **134**, 044128 (2011).
- [25] M. Lapert, R. Tehini, G. Turinici, and D. Sugny, Monotonically convergent optimal control theory of quantum systems under a nonlinear interaction with the control field, *Phys. Rev. A* **78**, 023408 (2008).
- [26] A. I. Konnov and V. A. Krotov, *Autom. Remote Control* **60**, 1427 (1999).
- [27] N. Khaneja, T. Reiss, C. Kehlet, T. Schulte-Herbrüggen, and S. J. Glaser, Optimal control of coupled spin dynamics: Design of NMR pulse sequences by gradient ascent algorithms, *J. Magn. Reson.* **172**, 296 (2005).
- [28] L. S. Pontryagin, V. G. Boltyanskii, R. V. Gamkrelidze, and E. F. Mishchenko, *The Mathematical Theory of Optimal Processes* (Wiley, New York, 1962).
- [29] U. Boscain, G. Charlot, J.-P. Gauthier, S. Guérin, and H. R. Jauslin, Optimal control in laser-induced population transfer for two- and three-level quantum systems, *J. Math. Phys.* **43**, 2107 (2002).
- [30] L. Van Damme, Q. Ansel, S. J. Glaser, and D. Sugny, Robust optimal control of two-level quantum systems, *Phys. Rev. A* **95**, 063403 (2017).

- [31] U. Boscain, M. Sigalotti, and D. Sugny, Introduction to the Pontryagin maximum principle for quantum optimal control, *PRX Quantum* **2**, 030203 (2021).
- [32] X. Chen, Y. Ban, and G. C. Hegerfeldt, Time-optimal quantum control of nonlinear two-level systems, *Phys. Rev. A* **94**, 023624 (2016).
- [33] J. Zeng, C. H. Yang, A. S. Dzurak, and E. Barnes, Geometric formalism for constructing arbitrary single-qubit dynamically corrected gates, *Phys. Rev. A* **99**, 052321 (2019).
- [34] G. Dridi, K. Liu, and S. Guérin, Optimal robust quantum control by inverse geometric optimization, *Phys. Rev. Lett.* **125**, 250403 (2020).
- [35] X. Laforgue, G. Dridi, and S. Guérin, Optimal robust quantum control against pulse inhomogeneities: Analytic solutions, *Phys. Rev. A* **106**, 052608 (2022).
- [36] P. D. Drummond and K. V. Kheruntsyan, Stimulated Raman adiabatic passage from an atomic to a molecular Bose-Einstein condensate, *Phys. Rev. A* **65**, 063619 (2002).
- [37] V. I. Arnold, V. V. Kozlov, and A. I. Neishtadt, *Mathematical Aspects of Classical and Celestial Mechanics*, 3rd ed. (Springer, Berlin, 2006).
- [38] J. Henrard, in *The Adiabatic Invariant Theory and Applications, in Hamiltonian Dynamics: Theory and Applications*, edited by G. Benettin, J. Henrard, S. B. Kuksin, and A. Giorgilli, Lecture Notes in Mathematics Vol. 1861 (Springer, Berlin, 2005).
- [39] A. P. Itin and S. Watanabe, Integrability, stability, and adiabaticity in nonlinear stimulated Raman adiabatic passage, *Phys. Rev. Lett.* **99**, 223903 (2007).
- [40] S. Guérin, M. Gevorgyan, C. Leroy, H. R. Jauslin, and A. Ishkhanyan, Efficient adiabatic tracking of driven quantum nonlinear systems, *Phys. Rev. A* **88**, 063622 (2013).
- [41] M. Gevorgyan, S. Guérin, C. Leroy, A. Ishkhanyan, and H. R. Jauslin, Adiabatic tracking for photo- and magneto-association of Bose-Einstein condensates with Kerr nonlinearities, *Eur. Phys. J. D* **70**, 253 (2016).
- [42] J. J. Zhu, X. Chen, H. R. Jauslin, and S. Guérin, Robust control of unstable nonlinear quantum systems, *Phys. Rev. A* **102**, 052203 (2020).
- [43] V. Dorier, M. Gevorgyan, A. Ishkhanyan, C. Leroy, H. R. Jauslin, and S. Guérin, Nonlinear stimulated Raman exact passage by resonance-locked inverse engineering, *Phys. Rev. Lett.* **119**, 243902 (2017).
- [44] T. Huang, B. A. Malomed, and X. Chen, Shortcuts to adiabaticity for an interacting Bose-Einstein condensate via exact solutions of the generalized Ermakov equation, *Chaos* **30**, 053131 (2020).
- [45] K. Efsthathiou, *Metamorphoses of Hamiltonian Systems with Symmetries*, Lecture Notes in Mathematics Vol. 1864 (Springer, Berlin, 2005).
- [46] N. V. Vitanov and B. W. Shore, Stimulated Raman adiabatic passage in a two-state system, *Phys. Rev. A* **73**, 053402 (2006).
- [47] J. C. Lagarias, J. A. Reeds, M. H. Wright, and P. E. Wright, Convergence properties of the Nelder-Mead simplex method in low dimensions, *SIAM J. Optim.* **9**, 112 (1998).
- [48] T.-N. Xu, K. Liu, X. Chen, and S. Guérin, Invariant-based optimal composite stimulated Raman exact passage, *J. Phys. B* **52**, 235501 (2019).